Supporting Information

***In-situ* Grown 2D Hydrated Ammonium Vanadate Nanosheets on Carbon Cloth as a Free-standing**

Cathode for High-performance Rechargeable Zn-ion Batteries

Hanmei Jiang[1], Yifu Zhang[*,1], Yanyan Liu[1], Jie Yang,[2] Lei Xu[1], Peng Wang[1], Zhanming Gao[1], Jiqi Zheng

[1], Changgong Meng[1], Zhenghui Pan[*,2]

[1]*School of Chemical Engineering, Dalian University of Technology, Dalian 116024, PR China*

[2]*Department of Materials Science and Engineering, National University of Singapore, 117574 Singapore,*

Singapore

*E-mail addresses: yfzhang@dlut.edu.cn (Y. Zhang); msepz@nus.edu.sg (Z. Pan)

Experimental section

Alkali treatment of CC

All chemicals purchased from Sinopharm Chemical Reagent Co., Ltd were with analytical grade and used without any further purification. Carbon cloth (CC) was purchased from Shanghai Lishuo Composite Material Technology Co., Ltd. Firstly, after immersed in 10% (wt) KOH aqueous for 3 h, the purchased CC was placed in tube furnace and kept at 900 °C for 3 h under the atmosphere of N_2. Then, CC was soaked in 1M HCl (aq) for 2 h and washed with deionized water thoroughly. The ACC was obtained through dried in oven at 60 °C for 12 h.

Synthesis of NV NSs@ACC

In a typical procedure, 4 mmol of NH_4VO_3 and 80 mL distilled water were mixed and magnetic stirred for a few minutes, after that 4 mmol of $H_2C_2O_4·2H_2O$ was added into the above solution. After stirred for 0.5 h at the room temperature, the homogeneous yellow solution was transferred into a sealed autoclave and maintained at 180 °C for 4 h. When the temperature was cooled down, the CC was washed liberally with distilled water and dried in oven at 60 °C for 12 h. The final product was denoted as NV NSs@ACC. And the sample of powder-formed NV active materials coated on ACC, denoted as NV-ACC.

Materials characterization

The phase and composition of the products were identified by X-ray powder diffraction (XRD, Panalytical X'Pert powder diffractometer at 40 kV and 40 mA with Ni-filtered Cu Kα radiation). X-ray photoelectron spectroscopy (XPS) was used to investigate the composition of the products and confirm the oxidation state of vanadium performed on ESCALAB250Xi, Thermo Fisher Scientific. The Raman spectra were obtained using a Thermo Scientific spectrometer, with a 532 nm excitation line. Fourier transform infrared spectroscopy (FTIR) pattern of the solid samples was measured using KBr pellet technique (About 1 wt. % of the samples and 99 wt. % of KBr were mixed homogeneously, and then the mixture was pressed to a pellet) and recorded on a Nicolet 6700 spectrometer from 4000 to 400 cm^{-1} with a resolution of 4 cm^{-1}. The morphology and dimensions of the products were observed by field emission scanning electron microscopy (FE-SEM, NOVA NanoSEM 450, FEI) and transmission electron microscopy (TEM, FEITecnai F30, FEI). The high-resolution transmission electron microscopy (HRTEM) and selected area

electron diffraction (SAED) were also carried out on FEITecnai F30. The samples were dispersed in absolute ethanol with ultrasonication before TEM characterization.

For the *ex-situ* XRD and XPS characterizations, the cycled electrodes were washed with deionized water and dried naturally in air. But as for the *ex-situ* SEM and STEM investigations, the cycled electrodes are ultrasound with alcohol.

Electrochemical characterization

Assembling coin-type batteries

CR2032 coin-type batteries were assembled by NV NSs@ACC as cathode directly (cut into wafers with the diameter of 12mm), Zn plate as anode, and glass fiber (Whatman GF/A) were employed as separator to test the electrochemical performance. A 3 M $Zn(CF_3SO_3)_2$ aqueous solution was used as the electrolyte. For comparison, NV NSs was synthesized (the XRD pattern is shown in Figure S2b) and another working electrode NV-ACC was fabricated by mixing NV NSs, a conductive agent (Super-P, Sigma-Aldrich), and PVDF (Sigma-Aldrich), in a weight ratio of 7 : 2 : 1. Next, the mixture was coated on CC. After drying in air at 90 °C for 12 h, the electrodes were used to fabricate the same CR2032 coin-type battery.

Assembling flexible devices

The $ZnSO_4$/CMC gel electrolytes were prepared by dissolving 20 g of $ZnSO_4 \cdot 7H_2O$ and 6 g of CMC in 160 mL of distilled water and heated at 85 °C for 120 min under vigorous stirring. The flexible devices were assembled by separating NV NSs@ACC and Zn NSs@CC (deposited Zn nanosheets on CC) with a separator and $ZnSO_4$/CMC gel electrolytes. Cyclic voltammetry (CV) and electrochemical impedance spectroscopy (EIS) were conducted on a CHI 660D electrochemical workstation. Galvanostatic charge-discharge (GCD) curves and cyclic performance were obtained through Wuhan LAND battery tester.
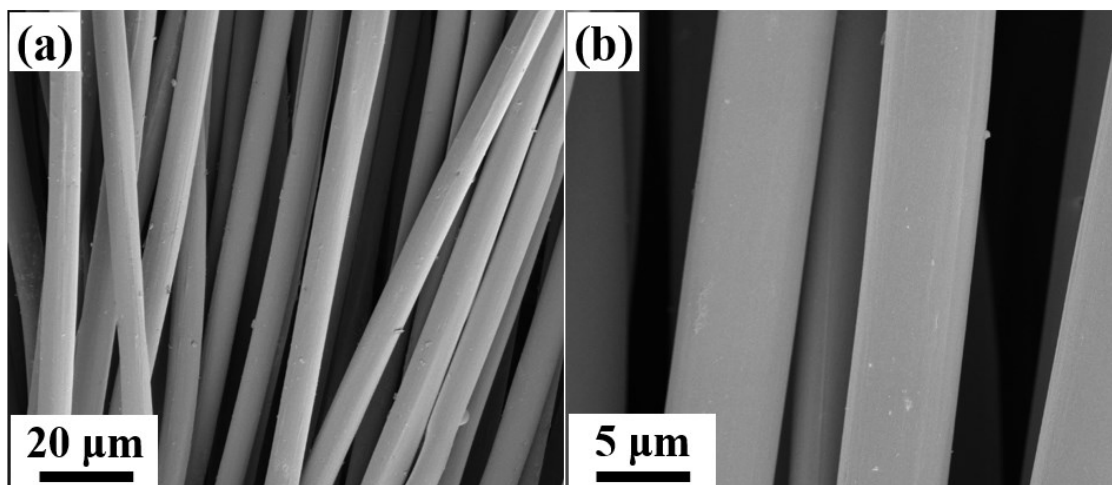
Figure S1

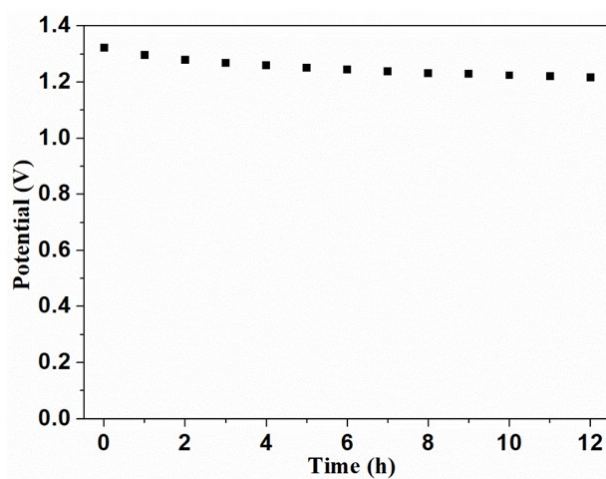Figure S1. SEM images of ACC substrates.

Figure S2

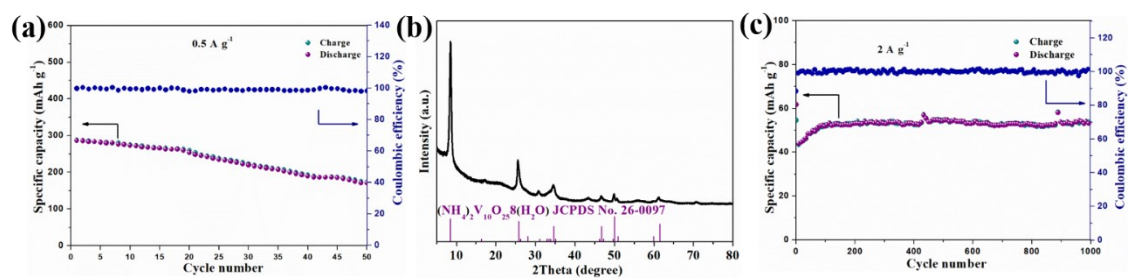Figure S2. Self-discharge curve of the battery during the standing process.

Figure S3

Figure S3. (a) Cycling performance of NV NSs@ACC at 0.5 A·g^{-1}. (b) XRD pattern of NV NSs. (c) Cycling performance of NV-ACC at 2 A·g^{-1}.
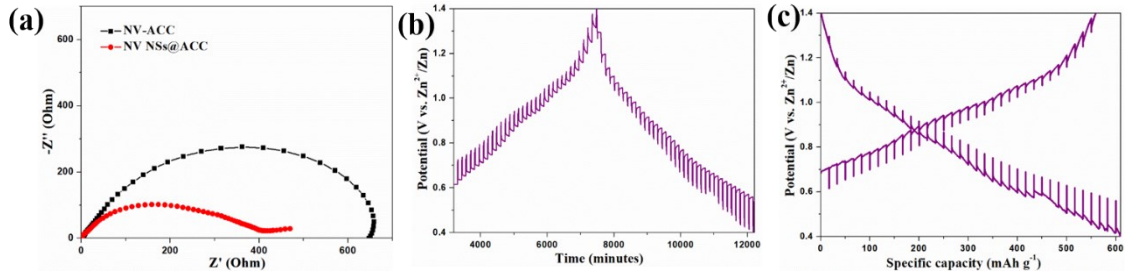
Figure S4

Figure S4. (a) EIS spectra of NV-ACC and NV NSs@ACC at pristine state. (b-c) Discharge/charge GITT profiles of NV NSs@ACC at 0.05 A g⁻¹.

Before the GITT measurement, the assembled cell was first discharged/charged at 100 mA g⁻¹ for 3 cycles to obtain a stable state. Subsequently, the cell was discharged or charged at 100 mA g⁻¹ for 20 min, and then relaxed for 110 min to make the voltage reach the equilibrium. The procedure was repeatedly applied to the cell during the entire charge/discharge process. The Zn^{2+} diffusion coefficient can be calculated based on the following equation [1, 2]:

$$D_{Zn^{2+}} = \frac{4}{\pi\tau}\left(\frac{m_B V_M}{M_B S}\right)^2\left(\frac{\Delta E_S}{\Delta E_\tau}\right)^2$$

where τ is the duration time of the current pulse, m_B is the mass of the active material, M_B is the molecular weight (g/mol) and V_M is its molar volume (cm³/mol), S is the total contacting area of electrode with electrolyte, ΔE_S and ΔE_τ are the change in the steady state voltage and overall cell voltage after the application of a current pulse in a single step GITT experiment, respectively.
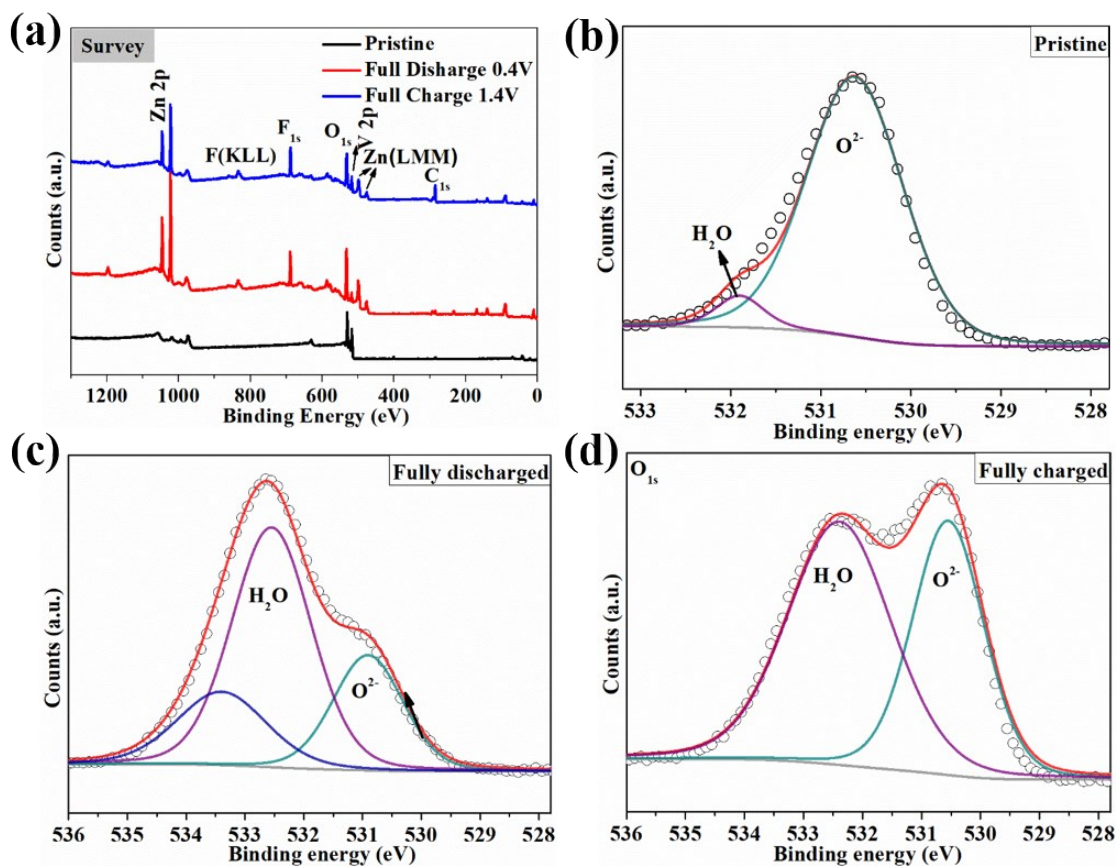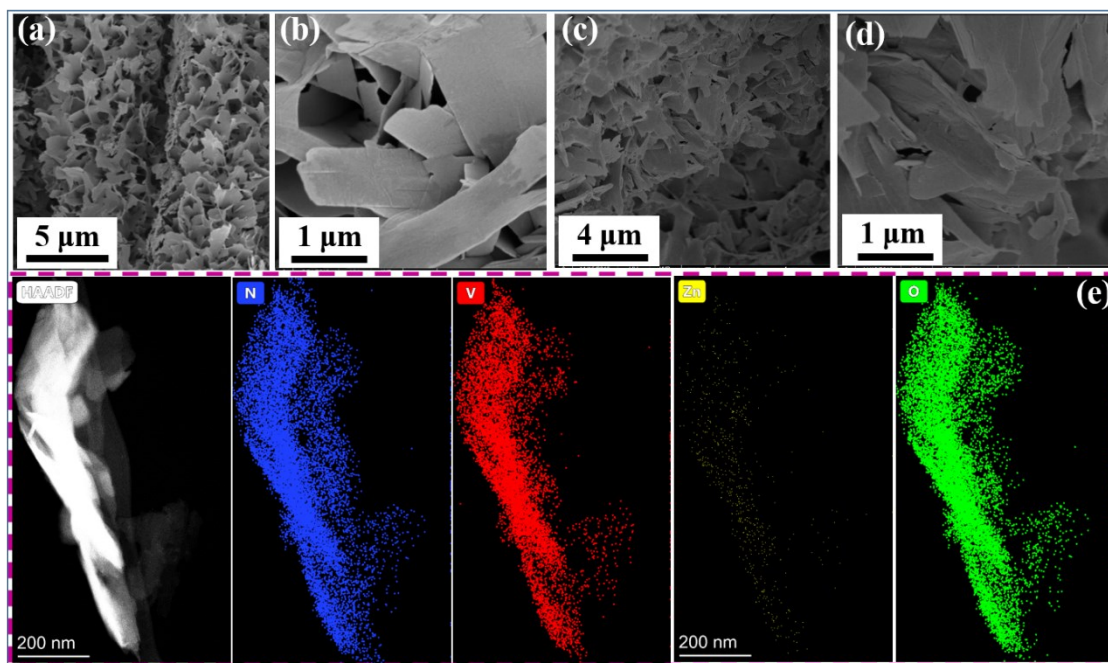
Figure S5

Figure S5. (a) *Ex-situ* XPS Survey spectra of NV NSs@ACC obtained at different states. (b-d) *Ex-situ* XPS O spectra of NV NSs@ACC obtained at different states.

Figures S5b-d depicts the O 1s XPS regions. In the pristine NV NSs@ACC electrode, two peaks observed at 530.6 and 531.9 eV are characteristics of the VO layers and the interlayer H_2O of $(NH_4)_2V_{10}O_{25}\cdot 8H_2O$. Upon discharge, the binding energy of 533.4 eV is attributed to the interactions between intercalated Zn^{2+} and the host materials[3]. The O 1s evolution re-emerges after fully charged.

Figure S6

Figure S6. (a-b) SEM images of NV NSs@ACC after 20 cycles at 0.1 A g^{-1}. (c-d) SEM images of NV NSs@ACC after 100 cycles at 2 A g^{-1}, and (e) The corresponding elemental mapping images (STEM) of NV NSs@ACC at 1.4 V.
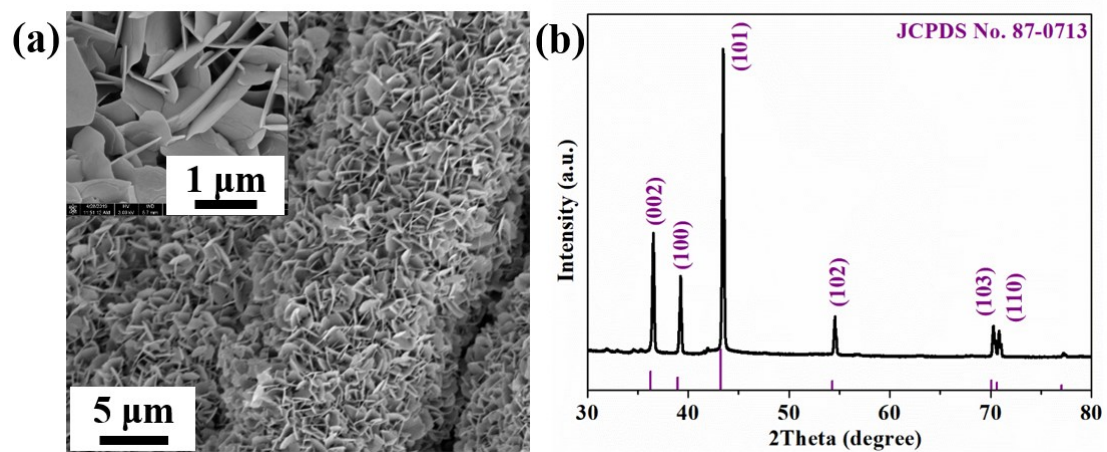
Figure S7

Figure S7. Zn NSs@CC: (a) SEM image. (b) XRD pattern.

Table S1

Table S1. Comparison of the performance between the previous powder-formed ammonium vanadate

based materials for ARZIBs and this work.

Cathode Materials	Approach of fabricating electrode	Specific capacity	Energy density	Power density	Ref.
NV NSs@ACC	**Directly used (Binder-free)**	**523 mAh g^{-1} at 0.1 A g^{-1}**	**422.5 Wh kg^{-1}** **342.7 Wh kg^{-1}**	**74.5 W kg^{-1}** **149.6 W kg^{-1}**	**This work**
$NH_4V_4O_{10}$	Active materials+ acetylene black+PVDF	380.3 mAh g^{-1} at 0.1 A g^{-1}	374.3 Wh kg^{-1}	9000 W kg^{-1}	[4]
$NH_4V_3O_8$	Active materials+ acetylene black+PVDF	~55 mAh g^{-1} at 0.5 A g^{-1}	NA	NA	[4]
$(NH_4)_2V_3O_8/C$	Active materials+ acetylene black+PVDF	356 mAh g^{-1} at 0.1 A g^{-1}	334 Wh kg^{-1}	294 W kg^{-1}	[5]
$(NH_4)_2V_{10}O_{25}\cdot8H_2O$	Active materials+ acetylene black+PVDF	228.8 mAh g^{-1} at 0.1 A g^{-1}	225.4 Wh kg^{-1}	NA	[3]
$(NH_4)_2V_{10}O_{25}\cdot8H_2O$	Active materials+ acetylene black+PVDF	417 mAh g^{-1} at 0.1 A g^{-1}	320 Wh kg^{-1}	77 W kg^{-1}	[6]
$NH_4V_4O_{10}$ nanobelt	Active materials+ carbon black+PVDF	147 mAh g^{-1} at 0.05 A g^{-1}	NA	NA	[7]
$(NH_4)_2V_6O_{16}\cdot1.5H_2O$	Active materials+ acetylene black+PVDF	479 mAh g^{-1} at 0.1 A g^{-1}	371.5 Wh kg^{-1}	3083 W kg^{-1}	[8]
$(NH_4)_2V_4O_9$	Active materials+ acetylene black+PVDF	376 mAh g^{-1} at 0.1 A g^{-1}	301 Wh kg^{-1}	197 W kg^{-1}	[9]
$NH_4V_4O_{10}$	Active materials+CNTs +PVDF	485 mAh g^{-1} at 0.1 A g^{-1}	321 Wh kg^{-1}	69 W kg^{-1}	[10]
$(NH_4)_2V_6O_{16}$	Active materials+ acetylene black+PVDF	323.3 mAh g^{-1} at 0.1 A g^{-1}	249 Wh kg^{-1}	98.8 W kg^{-1}	[11]
$NH_4V_3O_8\cdot0.5H_2O$	Active materials+ acetylene black+PVDF	423.3 mAh g^{-1} at 0.1 A g^{-1}	353 Wh kg^{-1}	114 W kg^{-1}	[12]

Table S2

Table S2. Comparison of the performance between the previous cathode materials for ARZIBs and this work.

Cathode Materials	Energy density	Power density	Ref.
NV NSs@ACC	**422.5 Wh kg^{-1}** **342.7 Wh kg^{-1}** **275.5 Wh kg^{-1}** **189.3 Wh kg^{-1}**	**74.5 W kg^{-1}** **149.6 W kg^{-1}** **301.5 W kg^{-1}** **796.1 W kg^{-1}**	**This work**
$Zn_2V_2O_7$ BDHSs/SWNT	185 Wh kg^{-1}	228 W kg^{-1}	[13]
$Ca_{0.25}V_2O_5 \cdot nH_2O$	267 Wh kg^{-1}	53.4 W kg^{-1}	[14]
a- $Zn_2V_2O_7$	87.3 Wh kg^{-1}	18.9 W kg^{-1}	[15]
$Na_2V_6O_{16} \cdot 3H_2O$ barnesite nanorod	90 Wh kg^{-1}	15800 W kg^{-1}	[16]
$K_2V_6O_{16} \cdot 2.7H_2O$ nanorods	128 Wh kg^{-1}	5760 W kg^{-1}	[17]
$VO_2(B)$ nanofibers	297 Wh kg^{-1}	180 W kg^{-1}	[18]
$VO_2(B)$ nanobelts	271.8 Wh kg^{-1}	NA	[19]
RGO/VO_2 composite	65 Wh kg^{-1}	7800 W kg^{-1}	[20]
$V_{10}O_{24} \cdot 12H_2O$	163.4 Wh kg^{-1}	217.9 W kg^{-1}	[21]
$V_2O_5 \cdot nH_2O$/graphene	144 Wh kg^{-1}	NA	[22]
VS_4@rGO	180 Wh kg^{-1}	145 W kg^{-1}	[23]
VS_2	123 Wh kg^{-1}	NA	[24]
The spaced V_2O_5	326 Wh kg^{-1}	92 W kg^{-1}	[25]

Table S3. Comparison of the calculated diffusion coefficient of Zn^{2+} between the previous cathode

materials for ARZIBs and this work.

Cathode Materials	Diffusion coefficient of Zn^{2+} $(cm^{-2}\ s^{-1})$	Ref.
NV NSs@ACC	**$10^{-9} \sim 10^{-10}$**	**This work**
V_2O_3	10^{-8}	[26]
VO-LGO	10^{-9} to 10^{-11}	[27]
$VO_2(D)$ hollow nanospheres	$10^{-8} \sim 10^{-10}$	[28]
V_2O_5	10^{-10} to 10^{-11}	[1]
$LiV_2(PO_4)_3$	10^{-13} to 10^{-14}	[29]
$K_2V_8O_{21}$	10^{-10} to 10^{-11}	[30]
$Fe_5V_{15}O_{39}(OH)_9 \cdot 9H_2O$	10^{-10} to 10^{-11}	[31]
$Na_2V_6O_{16} \cdot 1.63H_2O$	10^{-13}	[32]

Table S4. Changes about d-spacings of (001) plane in different samples corresponding to the *ex-situ* XRD patterns.

Samples	d-spacing (Å)
pristine	10.612
immerse in electrolyte for 1 h	13.205
cha. 1.4 V 1st	11.652
dis. 0.8 V 2nd	11.887
dis. 0.4 V 2nd	11.981
cha. 0.8 V 2nd	11.526
cha. 1.4 V 2nd	11.254

References

1. N. Zhang, Y. Dong, M. Jia, X. Bian, Y. Wang, M. Qiu, J. Xu, Y. Liu, L. Jiao and F. Cheng, *ACS Energy Lett.*, 2018, **3**, 1366-1372.

2. N. Zhang, F. Cheng, Y. Liu, Q. Zhao, K. Lei, C. Chen, X. Liu and J. Chen, *J. Am. Chem. Soc.*, 2016, **138**, 12894-12901.

3. T. Wei, Q. Li, G. Yang and C. Wang, *J. Mater. Chem. A*, 2018, **6**, 20402-20410.

4. B. Tang, J. Zhou, G. Fang, F. Liu, C. Zhu, C. Wang, A. Pan and S. Liang, *J. Mater. Chem. A*, 2019, **7**, 940-945.

5. H. Jiang, Y. Zhang, L. Xu, Z. Gao, J. Zheng, Q. Wang, C. Meng and J. Wang, *Chem. Eng. J.*, 2020, **382**, 122844.

6. H. Jiang, Y. Zhang, Z. Pan, L. Xu, J. Zheng, Z. Gao, T. Hu and C. Meng, *Electrochim. Acta*, 2020, **332**, 135506.

7. G. Yang, T. Wei and C. Wang, *ACS Appl. Mater. Interfaces*, 2018, **10**, 35079-35089.

8. X. Wang, B. Xi, Z. Feng, W. Chen, H. Li, Y. Jia, J. Feng, Y. Qian and S. Xiong, *J. Mater. Chem. A*, 2019, **7**, 19130-19139.

9. Y. Zhang, H. Jiang, L. Xu, Z. Gao and C. Meng, *ACS Appl. Energy Mater.*, 2019, **2**, 7861-7869.

10. Q. Li, X. Rui, D. Chen, Y. Feng, N. Xiao, L. Gan, Q. Zhang, Y. Yu and S. Huang, *Nano-Micro Lett.*, 2020, **12**, 67.

11. L. Xu, Y. Zhang, H. Jiang, J. Zheng, X. Dong, T. Hu and C. Meng, *Colloids and Surfaces A: Physicochemical and Engineering Aspects*, 2020, **593**, 124621.

12. H. Jiang, Y. Zhang, Z. Pan, L. Xu, J. Zheng, Z. Gao, T. Hu, C. Meng and J. Wang, *Mater. Chem. Front.*, 2020, **4**, 1434-1443.

13. F. Zhou, Y. Lin, T. Li, S. Zhang and C. Deng, *J. Mater. Chem. A*, 2019, **7**, 10589-10600.

14. C. Xia, J. Guo, P. Li, X. Zhang and H. N. Alshareef, *Angew. Chem. Int. Ed.*, 2018, **57**, 3943-3948.

15. B. Sambandam, V. Soundharrajan, S. Kim, M. H. Alfaruqi, J. Jo, S. Kim, V. Mathew, Y.-k. Sun and J. Kim, *J. Mater. Chem. A*, 2018, **6**, 3850-3856.

16. V. Soundharrajan, B. Sambandam, S. Kim, M. H. Alfaruqi, D. Y. Putro, J. Jo, S. Kim, V. Mathew, Y.-K. Sun and J. Kim, *Nano Lett.*, 2018, **18**, 2402-2410.

17. H. Li, Z. Liu, G. Liang, Y. Huang, Y. Huang, M. Zhu, Z. Pei, Q. Xue, Z. Tang, Y. Wang, B. Li and C. Zhi, *ACS Nano*, 2018, **12**, 3140-3148.

18. J. Ding, Z. Du, L. Gu, B. Li, L. Wang, S. Wang, Y. Gong and S. Yang, *Adv. Mater.*, 2018, **30**, 1800762.

19. T. Wei, Q. Li, G. Yang and C. Wang, *J. Mater. Chem. A*, 2018, **6**, 8006-8012.

20. X. Dai, F. Wan, L. Zhang, H. Cao and Z. Niu, *Energy Stor. Mater.*, 2019, **17**, 143-150.

21. T. Wei, Q. Li, G. Yang and C. Wang, *Electrochim. Acta*, 2018, **287**, 60-67.

22. M. Yan, P. He, Y. Chen, S. Wang, Q. Wei, K. Zhao, X. Xu, Q. An, Y. Shuang, Y. Shao, K. T. Mueller, L. Mai, J. Liu and J. Yang, *Adv. Mater.*, 2018, **30**, 1703725.

23. H. Qin, Z. Yang, L. Chen, X. Chen and L. Wang, *J. Mater. Chem. A*, 2018, **6**, 23757-23765.

24. P. He, M. Yan, G. Zhang, R. Sun, L. Chen, Q. An and L. Mai, *Adv. Energy Mater.*, 2017, **7**, 1601920.

25. X. Wang, L. Ma and J. Sun, *ACS Appl. Mater. Interfaces*, 2019, **11**, 41297-41303.

26. H. Luo, B. Wang, F. Wang, J. Yang, F. Wu, Y. Ning, Y. Zhou, D. Wang, H. Liu and S. Dou, *ACS Nano*, 2020, DOI: 10.1021/acsnano.0c02658.

27. T. Wei, Q. Li, G. Yang and C. Wang, *Adv. Energy Mater.*, 2019, **0**, 1901480.

28. L. Chen, Z. Yang and Y. Huang, *Nanoscale*, 2019, **11**, 13032-13039.

29. F. Wang, E. Hu, W. Sun, T. Gao, X. Ji, X. Fan, F. Han, X.-Q. Yang, K. Xu and C. Wang, *Energy Environ. Sci.*, 2018, **11**, 3168-3175.

30. B. Tang, G. Fang, J. Zhou, L. Wang, Y. Lei, C. Wang, T. Lin, Y. Tang and S. Liang, *Nano Energy*, 2018, **51**, 579-587.

31. Z. Peng, Q. Wei, S. Tan, P. He, W. Luo, Q. An and L. Mai, *ChemComm*, 2018, **54**, 4041-4044.

32. P. Hu, T. Zhu, X. Wang, X. Wei, M. Yan, J. Li, W. Luo, W. Yang, W. Zhang, L. Zhou, Z. Zhou and L. Mai, *Nano Lett.*, 2018, **18**, 1758-1763.